



# Phase diagram of the three-dimensional Anderson model for short-range speckle potentials

M. Pasek,<sup>1,2</sup> Z. Zhao,<sup>1</sup> D. Delande,<sup>2</sup> and G. Orso<sup>1</sup>

<sup>1</sup>Laboratoire Matériaux et Phénomènes Quantiques, Université Paris Diderot-Paris 7 and CNRS, UMR 7162, 75205 Paris Cedex 13, France

<sup>2</sup>Laboratoire Kastler Brossel, UPMC-Sorbonne Universités, CNRS, ENS-PSL Research University, Collège de France, 4 Place Jussieu, 75005 Paris, France

(Received 19 September 2015; published 18 November 2015)

We investigate the localization properties of atoms moving in a three-dimensional optical lattice in the presence of a disorder potential having the same probability distribution  $P(V)$  as laser speckles, and a spatial correlation length much shorter than the lattice spacing. We find that the disorder-averaged (single-particle) Green's function, calculated via the coherent-potential approximation, is in very good agreement with exact numerics. Using the transfer-matrix method, we compute the phase diagram in the energy-disorder plane and show that its peculiar shape can be understood from the self-consistent theory of localization. In particular, we recover the large asymmetry in the position of the mobility edge for blue and red speckles, which was recently observed numerically for spatially correlated speckle potentials.

DOI: [10.1103/PhysRevA.92.053618](https://doi.org/10.1103/PhysRevA.92.053618)

PACS number(s): 03.75.-b, 05.60.Gg, 05.30.Rt, 67.85.-d

## I. INTRODUCTION AND MODEL HAMILTONIAN

Recently, there has been a growth of experimental and theoretical studies [1] on Anderson localization of ultracold atoms exposed to disordered optical potentials, including quasiperiodic lattices and blue-detuned laser speckles. The latter behave quite differently from typical models of randomness considered for condensed-matter systems. Indeed, the potential distribution  $P(V)$  of blue speckles is not Gaussian but follows the exponential (Rayleigh) law [2,3]

$$P(V) = \frac{\Theta(V + V_0)}{V_0} \exp\left(-\frac{V + V_0}{V_0}\right), \quad (1)$$

where  $\Theta$  is the Heaviside function and  $V_0$  is the disorder strength. In Eq. (1), we have shifted the potential by its average value so that  $\bar{V} = 0$ . This distribution is bounded from below by  $-V_0$  and is asymmetric, implying that odd moments of the potential will be nonzero. The probability distribution of red-detuned potentials, which have not yet been implemented experimentally, is obtained by simply changing  $V$  to  $-V$  in Eq. (1). A second fundamental aspect of optical speckles is that they are spatially correlated, with a typical grain size of the order of  $1 \mu\text{m}$ .

Three different experiments [4–6] claimed the observation of three-dimensional (3D) Anderson localization of atoms exposed to blue speckles. However, the estimated mobility edge—namely, the critical value  $E = E_c$  of the energy separating localized ( $E < E_c$ ) from extended ( $E > E_c$ ) states—is in all cases larger (and even much larger in Ref. [6]) than the current theoretical and numerical predictions [7–11]. The question arises whether the problem is due to inadequate experimental measurements (it is, for example, very difficult to correctly analyze the density profiles after a relatively short time expansion in the presence of disorder [12]) or to incorrect theoretical predictions for the mobility edge.

From the theory side, exact numerical calculations of the mobility edge obtained via the transfer-matrix technique [7] have revealed a discrepancy with previous estimates based on the self-consistent theory of Anderson localization (SCTL) [9–11]. In particular, it was found that the on-site potential distribution is extremely important. Indeed, there is a large difference between blue-detuned speckles, where

the mobility edge is systematically negative (i.e., below the average potential), and red-detuned speckles, where it changes from negative at low  $V_0$  to positive at large  $V_0$  [7]. On the other hand, the details of the spatial correlation function—beyond the correlation length which fixes the characteristic quantum energy scale—do not play a major role. The aforementioned discrepancy with SCTL predictions originates most probably from the lack of accuracy in the calculation of the disorder-averaged single-particle Green's function, which is a fundamental ingredient of the SCTL approach. Indeed, in Refs. [9–11], this quantity has been computed within the self-consistent Born approximation (SCBA), which is by construction insensitive to the color of the speckle, and can only apply for a sufficiently weak disorder.

In this article we disentangle the role of the on-site potential distribution from the effects of spatial correlations by studying a spatially uncorrelated 3D Anderson model with a Rayleigh potential distribution. Our results cannot be directly compared to experiments which use a correlation length comparable to the atomic de Broglie wavelength, but they pinpoint the crucial importance of the asymmetric potential distribution which simple approximations such as the Born approximation (or its extension, the SCBA) are unable to capture.

We calculate the Green's function numerically, and show that the obtained results are well reproduced by the coherent-potential approximation (CPA), which takes into account the full statistical properties of the potential. The CPA self-energy is then injected in the SCTL to estimate the position of the mobility edge, which turns out to be in reasonably good agreement with the exact transfer-matrix calculations. It is worth mentioning that the CPA method has not yet been generalized to spatially correlated speckle potentials, although this generalization has been attempted for other types of spatially correlated disorder [13,14].

In first quantization, the 3D Anderson model is given by

$$H = \sum_{\langle ij \rangle} -J|i\rangle\langle j| + \sum_i V_i|i\rangle\langle i|, \quad (2)$$

where indices  $i, j$  label the sites of the lattice,  $J$  is the hopping term between nearest neighbors, and  $V_i$  is the random external potential. We choose the correlation length of the speckle

potential to be much shorter than the lattice spacing, so that we can assume the  $V_i$  values to be uncorrelated  $\overline{V_i V_j} = \langle V^2 \rangle \delta_{ij}$  and distributed according to Eq. (1). For larger values of the correlation length, the resulting lattice model becomes significantly more complicated than Eq. (2) (see Ref. [15]). For convenience, in the following we will use units  $J = 1$  and  $\hbar = 1$ .

For the specific case of the Anderson model, there is no need to study separately the blue- and red-detuned speckles. Indeed, the cubic lattice with nearest-neighbor coupling being bipartite, the sign of  $J$  is irrelevant and does not affect localization properties. As a consequence, the simultaneous change of all  $V_i \rightarrow -V_i$  is equivalent to reversing the sign of the Hamiltonian  $H \rightarrow -H$ . Since the former change turns a given realization of a blue-detuned speckle into a realization of a red-detuned speckle, all results obtained here for the blue speckle with the Rayleigh distribution, including the phase diagram, apply also to the red speckle under the change  $E \rightarrow -E$ , as shown in Fig. 2. In other words, by studying the two mobility edges around  $E = -6$  and  $E = +6$ , one covers both the blue- and red-detuned cases, respectively.

The plan of the paper is as follows. In Sec. II we present the exact phase diagram for the 3D Anderson model with the Rayleigh potential distribution, Eq. (1), obtained numerically via the transfer-matrix technique. In Sec. III we calculate the disorder-averaged single-particle Green's function numerically, and analytically using the CPA and the SCBA. The obtained results are then used in Sec. IV to estimate the position of the mobility edge via the SCTL and to compare it with the exact numerical results of Sec. II. Finally, we examine in Sec. V how our findings help to interpret numerical and experimental results for cold atoms in a continuous speckle potential.

## II. EXACT PHASE DIAGRAM

The transfer-matrix method consists in computing recursively the conductance of a bar with transverse section  $M \times M$  sites, and length  $L \gg M$ . The logarithm of the conductance (averaged over disorder realizations) decays linearly with the length of the bar, giving access to the quasi-one-dimensional (1D) localization length  $\lambda_M$ . The scaling theory of localization indicates that  $\lambda_M/M$  decreases with  $M$  in the localized regime, increases in the diffusive regime, and is constant for large  $M$  at the mobility edge [16]. The various  $\lambda_M/M$  versus energy curves—for various  $M$  values—thus cross at the critical energy, the mobility edge, as shown in Fig. 1. By gathering results at various values of the disorder strength  $V_0$ , we obtain the phase diagram of the Anderson model, shown in Fig. 2 for a blue-detuned speckle.

We note that the trajectory of the mobility edge behaves very differently at the two band edges. Indeed, starting from the left band edge of the clean model,  $E = -6$ , the mobility edge shifts to lower and lower energy as  $V_0$  increases until  $V_0 \approx 10$ , which is close to the critical disorder needed to localize all states. Since the potential distribution has a sharp cutoff at  $V = -V_0$ , there are strictly no states below  $E = -6 - V_0$ . In contrast, the spectrum is not bounded from above. At the right band edge,  $E = +6$ , however, the mobility edge moves only slightly to the right for very weak disorder, reaching  $E = 6.15$  at  $V_0 = 1$ , and then moves backward in a monotonous way.

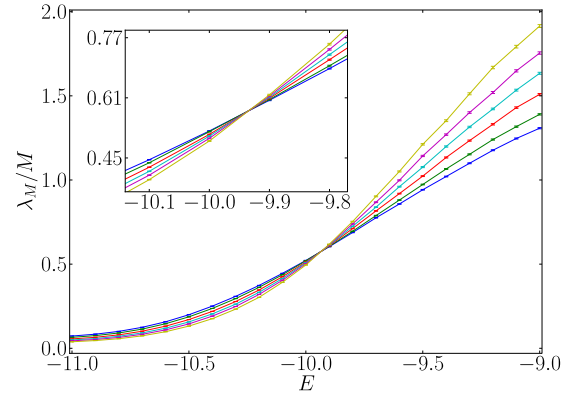


FIG. 1. (Color online) Transfer-matrix results for the 3D Anderson model with a spatially uncorrelated, blue-detuned speckle potential of strength  $V_0 = 8$ . Each curve displays the ratio of the localization length  $\lambda_M$  of a long bar with cross section  $M \times M$  to the bar transverse size  $M$ , as a function of energy. The various curves from  $M = 16$  (least steep curve) to  $M = 31$  (steepest curve) cross at the mobility edge  $E_c \approx -9.93$ .

This means that even for moderate disorder, starting from  $V_0 \approx 1$ , the asymmetry of the Rayleigh probability distribution  $P(V)$  becomes important and must be taken into account. This rules out the use of the SCBA for the calculation of the disorder-averaged Green's function, as we will show below.

## III. DISORDER-AVERAGED GREEN'S FUNCTION

In this section we calculate the disorder-averaged single-particle Green's function numerically, and analytically using two different approximation schemes, namely, the SCBA and the CPA. We also discuss two related quantities, the (disorder-averaged) density of states and the effective band edge (neglecting Lifshitz tails).

In the absence of disorder ( $V_0 = 0$ ), the Hamiltonian  $H$  becomes diagonal in momentum space,  $H = H_0 =$

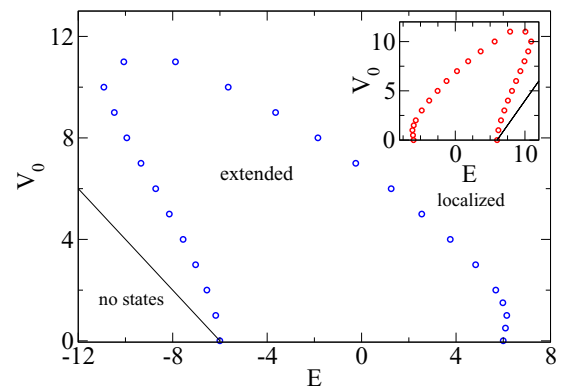


FIG. 2. (Color online) Exact localization phase diagram for the 3D Anderson model with a spatially uncorrelated, blue-detuned speckle potential obeying the Rayleigh distribution, Eq. (1), as obtained from the transfer-matrix technique and finite-size scaling. Notice that there are rigorously no states below the solid line corresponding to  $E = -6 - V_0$ . The phase diagram for red-detuned speckles is simply obtained under the change  $E \rightarrow -E$ , as shown in the inset.

$\sum_{\mathbf{k}} \epsilon(\mathbf{k})|\mathbf{k}\rangle\langle\mathbf{k}|$ , where  $\epsilon(\mathbf{k}) = -2(\cos k_x + \cos k_y + \cos k_z)$  is the energy dispersion of the atom in the cubic lattice. Hence, the diagonal part of the free-particle Green's function in the configuration-space representation  $G_0(E) \equiv \langle n|(E - H_0)^{-1}|n\rangle$  is translationally invariant and given by

$$G_0(E) = \int_{-\pi}^{\pi} \frac{d^3k}{(2\pi)^3} \frac{1}{E - \epsilon(\mathbf{k}) + i0}. \quad (3)$$

Following Joyce [17], we can express the unperturbed Green's function of a cubic lattice as  $G_0(E) = P(6/E)/E$ , where

$$P(z) = \frac{1 - 9\xi^4}{(1 - \xi)^3(1 + 3\xi)} \left[ \frac{2}{\pi} K(k_1) \right]^2. \quad (4)$$

Here,  $\xi$  and  $k_1$  are functions of  $z$  defined as

$$\xi(z) = \left( \frac{1 - \sqrt{1 - z^2/9}}{1 + \sqrt{1 - z^2}} \right)^{1/2}, \quad (5)$$

$$k_1(z)^2 = \frac{16\xi^3}{(1 - \xi)^3(1 + 3\xi)}, \quad (6)$$

and  $K$  is the complete elliptic integral of the first kind.

#### A. Numerical computation and analytical estimates of the self-energy

In the presence of a random potential, the translational symmetry is restored only after averaging over different realizations. The corresponding disorder-averaged Green's function is given by

$$\overline{G(E)} = \int_{-\pi}^{\pi} \frac{d^3k}{(2\pi)^3} \frac{1}{E - \epsilon(\mathbf{k}) - \Sigma(E, \mathbf{k})}, \quad (7)$$

where  $\Sigma = \Sigma' + i\Sigma''$  is the self-energy. The real part of the self-energy  $\Sigma'(E, \mathbf{k})$  represents how the energy of a plane wave with wave vector  $\mathbf{k}$  is shifted from  $\epsilon(\mathbf{k})$  ("renormalized") under the influence of the disorder, while the imaginary part  $\Sigma''(E, \mathbf{k})$ —which is always negative—yields the broadening of the energy distribution [18].

Numerically computing the self-energy is possible, but not completely straightforward. The starting point is the temporal representation of the Green's function as

$$\frac{1}{E - H + i0} = -i \int_0^{\infty} e^{-iHt} e^{iEt} dt. \quad (8)$$

As mentioned previously, the *average* Green's function in the presence of disorder is invariant by translation, i.e., diagonal in momentum space. Thus, one has

$$\begin{aligned} \overline{\langle \mathbf{k}|G(E)|\mathbf{k}\rangle} &= \frac{1}{E - \epsilon(\mathbf{k}) - \Sigma(E, \mathbf{k})} \\ &= -i \int_0^{\infty} \overline{\langle \mathbf{k}|e^{-iHt}|\mathbf{k}\rangle} e^{iEt} dt. \end{aligned} \quad (9)$$

The numerical calculation then amounts to propagating an initial plane wave  $|\mathbf{k}\rangle$  with the disordered Hamiltonian  $H$  during time  $t$  (with periodic boundary conditions) and to computing the overlap of the time-evolved state with  $|\mathbf{k}\rangle$ , followed by a Fourier transform from time to energy; subtracting  $E - \epsilon(\mathbf{k})$  from the inverse of the result yields the self-energy. This procedure is then repeated for several independent realizations

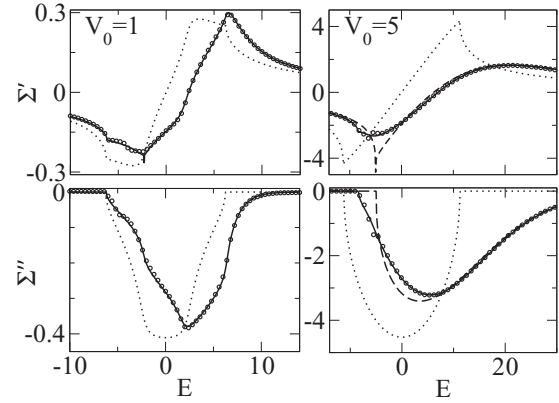


FIG. 3. Energy dependence of the real ( $\Sigma'$ ) and imaginary ( $\Sigma''$ ) parts of the self-energy calculated using the coherent-potential approximation [solid line, Eq. (12)] and the self-consistent Born approximation [dotted line, Eq. (11)] for two values of the disorder strength:  $V_0 = 1$  (left) and  $V_0 = 5$  (right). Also shown is the atomic limit approximation [dashed line, from Eqs. (15) and (16)] for  $V_0 = 5$ . In both cases, the CPA is a truly excellent approximation to the exact numerical results (for  $k = 0$ ) plotted as circles, reproducing almost all details of both the real and imaginary parts of the self-energy (note that for the numerical computations, system sizes of  $M^3$  with  $M = 28$  were used). In contrast, the SCBA is a rather poor approximation, even at a moderate disorder strength  $V_0 = 1$  where it is supposed to work best.

of the disorder to perform disorder averaging. In order to obtain small statistical fluctuations, a rather large number (of the order of  $10^5$ ) of disorder realizations is needed. Moreover, a sufficiently large system—much larger than the mean free path—has to be used to reduce finite-size effects. In our numerical results, we found that the self-energy has a very weak dependence on momentum, which is expected for spatially uncorrelated potentials,  $\overline{V_i V_j} = V_0^2 \delta_{ij}$ . In Fig. 3, we plot our numerical results for the real (upper panel) and imaginary (lower panel) parts of the self-energy, calculated at  $\mathbf{k} = \mathbf{0}$  for two different values of the disorder strength.

In the following, we compare our exact numerics with several approximate methods to calculate the self-energy. By construction, these methods yield estimates which are independent of momentum,  $\Sigma(E, \mathbf{k}) = \Sigma(E)$ . The simplest one is the Born approximation, which is given by

$$\Sigma(E) = V_0^2 G_0(E). \quad (10)$$

A slight, but simple, improvement is the self-consistent Born approximation (SCBA) where the disorder-free Green's function in Eq. (10) is modified self-consistently, leading to the equation

$$\Sigma(E) = V_0^2 G_0(E - \Sigma). \quad (11)$$

This quantity can be easily calculated numerically by successive iterations, starting from the Born approximation, Eq. (10). Since only the second moment of the potential distribution appears in the right-hand side (rhs) of Eq. (11), the SCBA self-energy *does not* depend on the details of the potential distribution  $P(V)$ , which makes sense only for sufficiently weak disorder.

A better approximation scheme at stronger disorder is given by the CPA [19]. The basic idea of the CPA is as follows (for a pedagogical discussion, see Ref. [20]): One isolates a single site  $i$  where the potential is chosen randomly according to  $P(V)$ , and replaces the surrounding sites by an effective homogeneous medium characterized by a uniform self-energy. One can then compute the single-site  $t$  matrix of site  $i$  embedded in the surrounding effective medium. The consistency condition is that the  $t$  matrix, averaged over the potential distribution at site  $i$ , vanishes; this translates into the self-consistent equation

$$\int P(V) \frac{V - \Sigma(E)}{1 - [V - \Sigma(E)]G_0(E - \Sigma(E))} dV = 0, \quad (12)$$

which clearly depends on the full probability distribution of the potential. For weak disorder, the CPA reduces to the SCBA, as is clear from Eq. (12) using the Taylor expansion  $1/(1-x) \simeq 1+x$ , with  $x = (V - \Sigma)G_0(E - \Sigma)$ . As the disorder strength increases, however, higher-order terms in the expansion become important and all moments of the potential distribution (cubic, quartic, etc.) will start to play a role. Hence, in general, the CPA yields more accurate results than the SCBA, as previously known for the Anderson model with a random-box potential [21,22]. By substituting the rhs of Eq. (1) in Eq. (12) and performing the integration over  $V$ , we obtain

$$e^{-u}[E_i(u) - i\pi] = gV_0, \quad (13)$$

where  $g = G_0(E - \Sigma)$ ,  $u = [1 + g(V_0 + \Sigma)]/(gV_0)$ , and  $E_i(u)$  is the exponential integral function defined as  $E_i(u) = -\text{P} \int_{-u}^{\infty} dt e^{-t}/t$ , with P being the principal value. Equation (13) can be easily solved numerically by a root-searching algorithm for the complex variable  $\Sigma$  or, again, by an iteration scheme.

The SCBA and CPA results for the self-energy are shown in Fig. 3 as dotted and solid lines, respectively. The most striking observation is that the CPA gives excellent predictions, almost in perfect agreement with our numerical results. Hence, this approximation can be safely used in the SCTL to compute the phase diagram of the Anderson model with a potential distribution typical of optical speckles. In contrast, the SCBA is a rather poor approximation, even at moderate disorder strength.

By construction, in the SCBA the real (imaginary) part of the self-energy is an odd (even) function of the energy and of the potential strength. We see in Fig. 3 that this feature disappears in the CPA, due to the asymmetry of the Rayleigh distribution, Eq. (1). In particular, for a fixed disorder strength, the imaginary part of the self-energy is much larger (in modulus) around  $E = 6$  as compared to  $E = -6$ , suggesting that disorder scattering is much stronger in red speckles.

The dependence of the self-energy on the speckle color is most evident in the atomic limit, either for  $V_0 \gg 1$  or  $E \gg 1$ , where all states are deeply localized. By neglecting the tunneling term in the Hamiltonian, one is left with a single-site problem. The disorder-averaged Green's function then takes the simple form

$$\overline{G(E)} = \int P(V) \frac{1}{E - V + i0} dV. \quad (14)$$

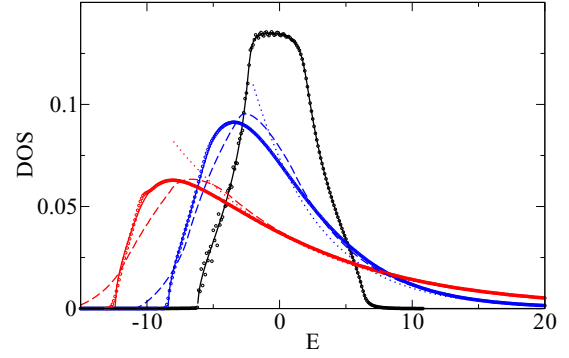


FIG. 4. (Color online) Density of states as a function of energy for three different values of the disorder strength  $V_0 = 1$  (black, first from the top at  $E = 0$ ),  $V_0 = 5$  (blue), and  $V_0 = 10$  (red). Dots correspond to the exact numerical results for system sizes  $M^3$  with  $M = 28$  (for  $V_0 = 1$ ), and  $M = 16$  (for  $V_0 = 5, 10$ ). The CPA predictions, shown as solid lines, are in excellent agreement with the numerical data, reproducing very well the existence of an effective band edge at low energy. Only some tiny features above the band edge are not correctly reproduced. The dashed lines correspond to the strong disorder (atomic limit) approximation, Eq. (17), and are reasonably accurate except near the low-energy effective band edge. The dotted lines are the large-energy asymptotic limit, Eq. (18).

By substituting the rhs of Eq. (1) in Eq. (14) and performing the integration over  $V$ , we find

$$\overline{G(E)} = \frac{1}{eV_0} \left[ f\left(\frac{E}{V_0}\right) - i\pi e^{-E/V_0} \Theta(E + V_0) \right], \quad (15)$$

where

$$f(x) = \text{P} \int_{-1}^{+\infty} \frac{e^{-z}}{x - z} dz. \quad (16)$$

The self-energy, calculated from Eqs. (15) and (16), is shown in Fig. 3 for  $V_0 = 5$  as a dashed line, and we see that it agrees with the exact numerics at high energies.

We stress that the exact energy spectrum is bounded from below by  $E = -6 - V_0$ , which implies that the imaginary part of the self-energy ( $\Sigma''$ ) is strictly zero below this value. However, numerical results show that there are very few states immediately above  $E = -6 - V_0$ , in the so-called Lifshitz tail, where  $\Sigma''$  is extremely small. It only raises at a significantly larger energy  $E \approx -8.4$  for  $V_0 = 5$  (while  $-6 - V_0 = -11$ )—see Fig. 3 or Fig. 4 below. Thus, there is an effective band edge which is higher than the rigorous band edge. Both the SCBA and the CPA, being insensitive to Lifshitz tails, have a band edge below which  $\Sigma''$  vanishes. We see in Fig. 3 that the CPA band edge is in excellent agreement with exact numerics, while the SCBA band edge is displaced towards negative energies.

## B. Density of states and band edge

In Fig. 4 we plot the averaged density of states (DOS)  $\rho = -\text{Im} \overline{G(E)}/\pi$  calculated within the CPA for increasing values of the disorder strength, compared to exact numerical values obtained from the self-energy using Eq. (7). Again, the agreement between the CPA and exact numerics is very good. As disorder increases, the peak in the DOS shifts towards

negative energies and becomes strongly asymmetric [23]. In particular, the DOS develops exponential tails [decaying as  $\exp(-E/V_0)$ ] at high energies, whereas at negative energies it vanishes more and more sharply with increasing  $V_0$ . In the atomic limit  $V_0 \gg 1$ , the density of states has been computed in Ref. [23] [Eq. (19)] and is simply given by the convolution of the disorder-free density of states  $\rho_0(E)$  by the on-site potential distribution, Eq. (1):

$$\rho(E) = \int \rho_0(x)P(E-x)dx. \quad (17)$$

For  $V_0 \gg 1$ , the width of the disorder-free band (energy range  $[-6, +6]$ ) is negligibly small, and we obtain

$$\rho(E) = \frac{1}{eV_0} e^{-E/V_0} \Theta(E+V_0), \quad (18)$$

in agreement with Eq. (15). At high energy, the convolution, Eq. (17), reduces to the simple exponential tail, Eq. (18). In Fig. 4, we show the numerically computed density of states compared to the prediction of Eq. (17), and its high-energy asymptotic limit, Eq. (18). While the agreement is fair even down to moderate values of the disorder strength (such as  $V_0 = 5$ ), some deviations exist near the low-energy effective band edge, as discussed in Ref. [23]. We mention that the density of states of atoms in spatially correlated speckle potentials has been studied both numerically and analytically in one dimension [24].

We now turn our attention to the effective band edge and derive analytical formulas for the SCBA and the CPA predictions for weak disorder. The unperturbed Green's function is first expanded around the unperturbed band edge  $E = -6$ , yielding  $G_0(E) = G_0(-6 + \tilde{E}) \simeq A + B\sqrt{-\tilde{E}}$ , where  $A = G_0(-6) = (14\sqrt{6} + 20\sqrt{3} - 24\sqrt{2} - 36)K^2$  ( $(2-\sqrt{3})(\sqrt{3}-\sqrt{2})/\pi^2 \approx -0.252731$ ) and  $B = 1/(4\pi) \approx 0.079577$ . Substituting this expression in Eq. (11) gives the self-consistent equation

$$\Sigma = V_0^2(A + B\sqrt{\Sigma - \tilde{E}}). \quad (19)$$

For weak disorder, we can replace the self-energy in the rhs of Eq. (19) by its leading term,  $\Sigma = V_0^2 A$ , which is real. As a consequence, the self-energy can only become complex if the argument of the square root in Eq. (19) becomes negative, that is,  $\tilde{E} = \Sigma$ . This means that the SCBA band edge is given by  $E_{\text{BE}}^{\text{SCBA}} = -6 + AV_0^2 + O(V_0^4)$ . It is possible to get the next order term—note that by construction of SCBA, only even powers of  $V_0$  appear—by using Eq. (19). By bringing the term proportional to  $A$  to the left-hand side (lhs) and taking the square of both sides, we find that  $\Sigma$  satisfies the following quadratic equation:

$$\Sigma^2 - (2AV_0^2 + B^2V_0^4)\Sigma + A^2V_0^4 + B^2V_0^4\tilde{E} = 0. \quad (20)$$

The band edge then corresponds to the energy value at which the discriminant vanishes. This gives

$$E_{\text{BE}}^{\text{SCBA}} = -6 + AV_0^2 + \frac{B^2}{4}V_0^4 + O(V_0^6), \quad (21)$$

which is shown in Fig. 5 with the red solid line.

Let us now focus on the CPA band edge. By setting  $z = gV_0$ ,  $y = g\Sigma$ , and  $x = V/V_0$ , the self-consistent Eq. (12) for the

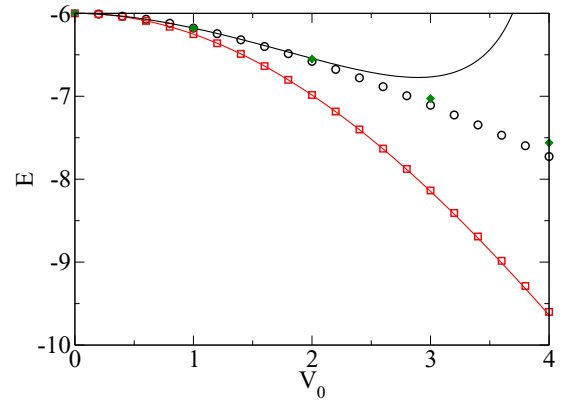


FIG. 5. (Color online) Band edge  $E_{\text{BE}}$  plotted as a function of disorder strength, calculated within the SCBA (red squares) and the CPA (black circles). Solid lines refer to the corresponding approximate analytical expressions, Eqs. (21) and (26), obtained for weak disorder. The exact transfer-matrix results for the mobility edge are also shown (green diamonds).

CPA self-energy can be written as

$$y = \frac{z}{e} \int_{-1}^{+\infty} \frac{e^{-x}x}{1-xz+y} dx. \quad (22)$$

The argument in the integral is expanded in powers of  $y$  up to the quadratic term,

$$y \simeq \frac{z}{e} \int_{-1}^{+\infty} e^{-x}x \left( \frac{1}{1-xz} - \frac{y}{(1-xz)^2} + \frac{y^2}{(1-xz)^3} \right) dx = f_0(z) + f_1(z)y + f_2(z)y^2, \quad (23)$$

where  $f_i(z)$  are functions of  $z$  defined in the interval  $[-1, 0]$ . For small values of  $z$ ,  $f_2(z) \simeq z^2$ , implying that  $y = F(z) + O(z^6)$ , where

$$F(z) = \frac{f_0(z)}{1 - f_1(z)}. \quad (24)$$

By inserting the asymptotic expansion of the Green's function  $g \simeq A + B\sqrt{\Sigma - \tilde{E}}$  in the formula  $\Sigma \simeq F(gV_0)/g$  and Taylor-expanding the rhs, we find with the same level of accuracy that

$$\Sigma \simeq \frac{F(AV_0) + F'(AV_0)BV_0\sqrt{\Sigma - \tilde{E}}}{A + B\sqrt{\Sigma - \tilde{E}}}. \quad (25)$$

Repeating the same procedure as above, we obtain the following approximate formula for the CPA band edge:

$$E_{\text{BE}}^{\text{CPA}} = -6 + \frac{F(AV_0)}{A} + \left[ \frac{F'(AV_0)V_0}{A} - \frac{F(AV_0)}{A^2} \right]^2 \frac{B^2}{4} + O(V_0^6). \quad (26)$$

This formula, shown in Fig. 5 with the black solid line, reproduces very well the numerical results (open circles) for the CPA band edge at small disorder. By using the Taylor expansion  $F(z) = z^2 + 2z^3 + 7z^4 + 34z^5 + O(z^6)$ , one can

obtain the expansion of the CPA band edge in powers of  $V_0$ :

$$E_{\text{BE}}^{\text{CPA}} = -6 + AV_0^2 + 2A^2V_0^3 + \left(\frac{B^2}{4} + 7A^3\right)V_0^4 + (2AB^2 + 34A^4)V_0^5 + O(V_0^6). \quad (27)$$

Note that odd-power terms, which are absent in the SCBA, appear due to the asymmetry of the Rayleigh potential distribution, and that the fourth-order term in Eq. (27) is different from the SCBA result, Eq. (21).

#### IV. SELF-CONSISTENT THEORY OF ANDERSON LOCALIZATION

Starting from the weak-localization corrections to the conductivity (or to the diffusion constant), the SCTL provides a useful microscopic justification of the Ioffe-Regel criterion  $k\ell \approx C$  for the onset of localization in 3D continuous models,  $C$  being a model-dependent constant of order unity. Both the wave number  $k$  and mean free path  $\ell$  depend on the energy  $E$ , but not in any simple way. Indeed, the usual relation—in the absence of disorder—between  $k$  and  $E$ ,  $E = \epsilon(\mathbf{k})$  is no longer correct in the vicinity of the mobility edge (strong-scattering regime), and there is no unique way of defining  $k(E)$  and  $\ell(E)$ . In the simplest approximation, one may assume that the dominant effect of strong disorder is to shift the band edge and dispersion relation by the real part of the self-energy  $\Sigma'$ , so that, for example,  $k(E)$  is nothing but  $k_0(E - \Sigma'(E))$ , where the “0” subscript refers to disorder-free quantities. As for the broadening of the spectral function (related to the imaginary part  $\Sigma''$ ), it is approximately symmetric and thus expected to have a negligible effect on averaged quantities. For lattice models, which have an anisotropic dispersion relation,  $k$  becomes a vector quantity so that the Ioffe-Regel criterion cannot be used straightforwardly. A simple generalization has been proposed in Ref. [25] that reads

$$S_0(E - \Sigma')\ell(E)^2 = 4\pi C^2, \quad (28)$$

where  $S_0(E)$  is the area of the surface  $\epsilon(\mathbf{k}) = E$  in momentum space,

$$S_0(E) = \int |\nabla_{\mathbf{k}}\epsilon| \delta(E - \epsilon(\mathbf{k})) d^3k. \quad (29)$$

The mean free path can be written as  $\ell(E) \sim v(E)\tau(E)$ , where  $v(E) = v_0(E - \Sigma')$  is the average modulus of the particle velocity, defined as

$$v_0(E) = \frac{1}{S_0(E)} \int |\nabla_{\mathbf{k}}\epsilon|^2 \delta(E - \epsilon(\mathbf{k})) d^3k, \quad (30)$$

and  $\tau(E)$  is the relaxation time due to disorder, which is related to the imaginary part of the self-energy as

$$\tau = -\frac{1}{2\Sigma''}. \quad (31)$$

Then Eq. (28) reduces to

$$\frac{S_0(E - \Sigma')v_0(E - \Sigma')^2}{\Sigma''^2} = 16\pi C^2. \quad (32)$$

Note that for continuous systems with a “massive” dispersion relation,  $E = k^2/2m$ , one has  $S_0(E) = 8\pi mE$  and  $v_0(E) =$

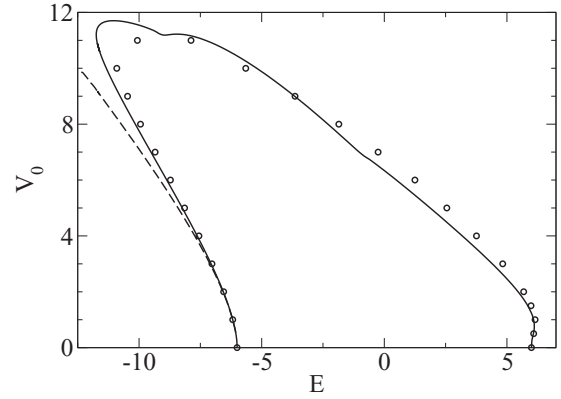


FIG. 6. Prediction of the self-consistent theory of localization—see Eq. (32)—for the mobility edge of the Anderson model with a Rayleigh potential distribution, using the CPA self-energy (solid line). The open circles correspond to the transfer-matrix results of Fig. 2. The dashed line represents the band edge calculated from CPA, neglecting Lifshitz tails.

$k_0/m = \sqrt{2E/m}$ , so that Eq. (32) indeed reduces to the Ioffe-Regel criterion.

Equations (29), (30), and (32) allow one to extract the complete phase diagram of the Anderson model once the CPA self-energy has been computed from Eq. (12), and a reasonable choice for the constant  $C$  in Eq. (32) has been made. For the random-box potential distribution,  $P_{\text{box}}(V) = \Theta(W/2 - V)/W$ , this constant was chosen [25] to reproduce the well-known transfer-matrix result  $W = W_c = 16.5$  for the critical disorder strength at the center of the band ( $E = 0$ ). Inserting the box distribution in Eq. (12) for the CPA self-energy, one obtains  $\Sigma_{\text{box}}(E = 0) = 0 - i4.7011$  for  $W = 16.5$ , which yields, using Eq. (32), the constant  $C_{\text{box}} = 0.775$ . For definiteness, we will calculate the mobility edge for the spatially uncorrelated speckle potential using the same constant, that is, we set  $C = C_{\text{box}}$ . Other choices of the constant will produce qualitatively similar results.

In Fig. 6, we compare the SCTL predictions (solid line) with the transfer-matrix results obtained in Sec. II. We see that the SCTL reproduces the overall shape of the exact phase diagram. In particular, the generalized Ioffe-Regel criterion, Eq. (32), provides a natural explanation for the behavior of the mobility edge at positive energies. Indeed, we see from Fig. 3 that near  $E = 6$  the imaginary part of the self-energy  $\Sigma''$  is rather large, or equivalently, the relaxation time in Eq. (31) is rather short. As a consequence,  $S_0(E - \Sigma')$  must therefore increase, which means that  $E_c$  will move towards the center of the band, where  $S_0(E)$  takes its maximum value,  $S_0(0) = 92.8756$ .

In Fig. 6, one can also see cusps in the SCTL mobility edge occurring at  $E = -9.14$  for  $V_0 = 11.22$  and, although it is less evident, at  $E = -0.83$  for  $V_0 = 6.86$ . These features are related to the presence of Van Hove singularities [26] in the DOS of the *clean* system at  $E = \pm 2$ . Indeed, at the cusp positions, the real part of the self-energy satisfies  $E - \Sigma' = -2$  and  $E - \Sigma' = 2$ , respectively.

Another interesting feature of Fig. 6 is that the mobility edge at negative energies remains very close to the CPA band edge, even for moderate disorder. This can be easily understood:

In the immediate vicinity of the effective band edge  $E_{\text{BE}}^{\text{CPA}}$ , the density of states and dispersion relation are very similar to the ones of the disorder-free system near the disorder-free band edge  $E = -6$ , meaning that they can be obtained from the disorder-free quantities by the shift  $E \rightarrow E - E_{\text{BE}}$ , where  $E_{\text{BE}} = E_{\text{BE}}^{\text{CPA}}$ . This shift is slightly different from the one in Eq. (32), i.e., using  $\Sigma'$ , although the two quantities coincide up to order  $V_0^4$  (see above). Using  $E_{\text{BE}}$  is a better approximation, however, as it ensures that the density of states exactly vanishes at  $E = E_{\text{BE}}$ . Thus, close to the effective band edge, one has approximately the average velocity (the effective mass of the Anderson model is  $m = 1/2$ )

$$v_0(E - E_{\text{BE}}) \simeq 2k(E), \quad (33)$$

with  $k(E) = \sqrt{E - E_{\text{BE}}}$ , whereas the area of the constant-energy shell is

$$S_0(E - E_{\text{BE}}) \simeq 4\pi k(E)^2. \quad (34)$$

It also follows that the imaginary part of the self-energy in the Born approximation, Eq. (10), behaves as

$$\Sigma''(E) = -\frac{V_0^2 k(E)}{4\pi}. \quad (35)$$

This is in agreement with the square-root behavior of  $\Sigma''(E)$  above the CPA band edge observed in Fig. 3. It also means that at low energy the mean free path is proportional to  $1/V_0^2$  and independent of energy. Inserting Eqs. (33)–(35) in the generalized Ioffe-Regel criterion, Eq. (32), yields

$$E_c - E_{\text{BE}} = \left(\frac{CV_0^2}{4\pi}\right)^2. \quad (36)$$

Therefore, in the weak disorder limit  $V_0 \ll 1$ , the effective band edge is shifted to the left of  $E = -6$  proportionally to  $V_0^2$ , while the distance to the mobility edge is much smaller, scaling as  $V_0^4$ .

## V. CONSEQUENCES FOR ANDERSON LOCALIZATION OF COLD ATOMS

A direct implementation of the spatially uncorrelated 3D Anderson model with cold atoms would require one to create a tight cubic optical lattice so that only the first band is populated, an ultracold gas so that  $k_B T$  is much smaller than the bandwidth (proportional to the tunneling rate between neighboring sites), and a speckle potential with a correlation length much shorter than the lattice spacing. Meeting all these requirements in current experiments seems rather difficult.

From the present study, one can nevertheless draw a few conclusions about the Anderson localization of massive particles in realistic optical speckles, as realized in recent experiments. Because of finite-range correlations, the disorder strength  $V_0$  must be compared to the other characteristic energy scale, namely, the “quantum” correlation energy  $E_\sigma = \hbar^2/m\sigma^2$ ,  $\sigma$  being the correlation length. A thorough discussion of the various possible regimes can be found in Ref. [3]. Especially, the effective band edge and the distance of the mobility edge to the effective band edge were found to scale as  $V_0^2$  and  $V_0^4$ , respectively, in agreement with our results (with, however, a caveat—see below). In the “quantum”

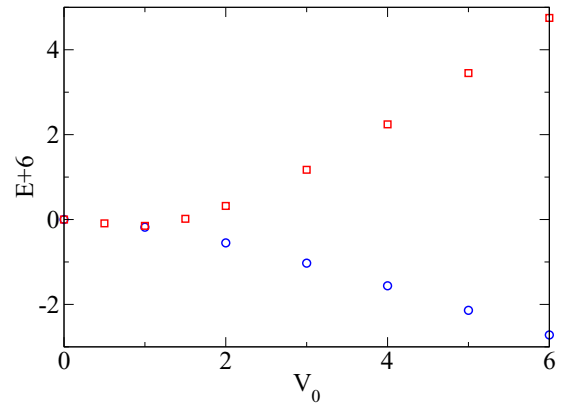


FIG. 7. (Color online) Zoom-in of the phase diagram (see Fig. 2) for blue (circles) and red (squares) speckles at the bottom of the band. The shape is qualitatively similar to the one obtained for spatially correlated speckles in Ref. [7], pointing out the crucial role played by the on-site potential distribution  $P(V)$ .

regime,  $V_0 \ll E_\sigma$ , the de Broglie wavelength of the particle is much larger than the correlation length of the potential, and it is reasonable to expect speckles to essentially behave as  $\delta$ -correlated potentials. Very recent unpublished work [27] shows that the phase diagram for atoms in an optical lattice exposed to an additional speckle potential with a correlation length shorter, but not *much* shorter, than the lattice spacing is qualitatively very similar to our result.

In Fig. 7 we reproduce the portion of the phase diagram near  $E = -6$ , calculated in Sec. II for blue and red speckle potentials. Because of the above-mentioned symmetry between the phase diagrams of blue- and red-detuned speckles under the transformation  $E \rightarrow -E$ , the red points are nothing but the data of Fig. 2 near  $E = +6$  for a blue-detuned speckle, with the sign of the energy reversed. Several features of previous numerical calculations [7] for speckle potentials with isotropic correlations are recovered:

- (i) At very low  $V_0 \ll E_\sigma$ , for both blue- and red-detuned speckles, the mobility edge lies below the average potential.
- (ii) For larger  $V_0$  and blue-detuned speckle, the mobility edge goes to lower and lower energy.
- (iii) In contrast, for a red-detuned speckle, the mobility edge has a turning point and becomes larger than the average potential energy.

However, we stress that a strict mapping of the Anderson model on the behavior of a massive particle is not possible for realistic speckle potentials. Indeed, as discussed in Ref. [3], the correlation function of the speckle potential has a long-range tail (decreasing not faster than  $1/r^2$  at a large distance). As a result, the integral of the correlation function diverges, implying that the “white-noise” limit, which could be associated with a purely uncorrelated potential, does not exist. Thus, even if the qualitative behaviors are similar, quantitative differences are expected.

## VI. SUMMARY AND CONCLUSION

In conclusion, we have carried out a thorough analysis of the 3D Anderson model for spatially uncorrelated

random potentials, i.e., potentials with a correlation length much shorter than the lattice spacing, obeying the Rayleigh probability distribution Eq. (1). We have shown that the asymmetry in the mobility edge of cold atoms exposed to blue and red speckles, as recently found numerically in spatially correlated isotropic potentials [7], is directly related to the asymmetry of the Rayleigh distribution under the change  $V \rightarrow -V$ . Finally, our work points out the crucial importance of a correct evaluation of the single-particle Green's function in speckle potentials, as a necessary condition to apply the self-consistent theory of localization. We hope that our results will stimulate further work to generalize the coherent-

potential approximation to spatially correlated speckle potentials.

#### ACKNOWLEDGMENTS

This work has been supported by the Region Ile-de-France in the framework of DIM Nano-K. The authors were granted access to the HPC resources of TGCC under the allocations 2014-057301, 2015-05730, and 2015-057083 made by GENCI ("Grand Equipement National de Calcul Intensif"). D.D. thanks Cord Müller for useful discussions, comments, and suggestions.

- 
- [1] L. Sanchez-Palencia and M. Lewenstein, *Nat. Phys.* **6**, 87 (2010).
  - [2] J. Goodman, *Speckle Phenomena in Optics: Theory and Applications* (Roberts & Company, Greenwood Village, CO, 2007).
  - [3] B. Shapiro, *J. Phys. A* **45**, 143001 (2012).
  - [4] F. Jendrzejewski, A. Bernard, K. Müller, P. Cheinet, V. Josse, M. Piraud, L. Pezzé, L. Sanchez-Palencia, A. Aspect, and P. Bouyer, *Nat. Phys.* **8**, 398 (2012).
  - [5] G. Semeghini, M. Landini, P. Castilho, S. Roy, G. Spagnolli, A. Trenkwalder, M. Fattori, M. Inguscio, and G. Modugno, *Nat. Phys.* **11**, 554 (2015).
  - [6] S. S. Kondov, W. R. McGehee, J. J. Zirbel, and B. DeMarco, *Science* **334**, 66 (2011).
  - [7] D. Delande and G. Orso, *Phys. Rev. Lett.* **113**, 060601 (2014).
  - [8] E. Fratini and S. Pilati, *Phys. Rev. A* **91**, 061601 (2015).
  - [9] R. Kuhn, O. Sigwarth, C. Miniatura, D. Delande, and C. Müller, *New J. Phys.* **9**, 161 (2007).
  - [10] M. Piraud, L. Pezzé, and L. Sanchez-Palencia, *New J. Phys.* **15**, 075007 (2013).
  - [11] A. Yedjour and B. A. Tiggelen, *Eur. Phys. J. D* **59**, 249 (2010).
  - [12] C. A. Müller and B. Shapiro, *Phys. Rev. Lett.* **113**, 099601 (2014).
  - [13] T. Maier, M. Jarrell, T. Pruschke, and M. H. Hettler, *Rev. Mod. Phys.* **77**, 1027 (2005).
  - [14] R. Zimmermann and C. Schindler, *Phys. Rev. B* **80**, 144202 (2009).
  - [15] S. Q. Zhou and D. M. Ceperley, *Phys. Rev. A* **81**, 013402 (2010).
  - [16] A. McKinnon and B. Kramer, *Z. Phys. B* **53**, 1 (1983).
  - [17] G. S. Joyce, *J. Phys. A* **31**, 5105 (1998).
  - [18] G. D. Mahan, *Many-Particle Physics*, 2nd ed. (Plenum, New York, 1993).
  - [19] R. J. Elliott, J. A. Krumhansl, and P. L. Leath, *Rev. Mod. Phys.* **46**, 465 (1974).
  - [20] G. Rickayzen, *Green's Functions and Condensed Matter* (Dover, New York, 2013).
  - [21] J. Kroha, T. Kopp, and P. Wölfle, *Phys. Rev. B* **41**, 888 (1990).
  - [22] J. Kroha, *Physica A* **167**, 231 (1990).
  - [23] M. I. Trappe, D. Delande, and C. A. Müller, *J. Phys. A* **48**, 245102 (2015).
  - [24] G. M. Falco, A. A. Fedorenko, J. Giacomelli, and M. Modugno, *Phys. Rev. A* **82**, 053405 (2010).
  - [25] E. N. Economou, C. M. Soukoulis, and A. D. Zdetsis, *Phys. Rev. B* **30**, 1686 (1984).
  - [26] L. Van Hove, *Phys. Rev.* **89**, 1189 (1953).
  - [27] E. Fratini and S. Pilati, [arXiv:1510.05121](https://arxiv.org/abs/1510.05121).